Supplement of Biogeosciences, 22, 6861–6875, 2025 https://doi.org/10.5194/bg-22-6861-2025-supplement © Author(s) 2025. CC BY 4.0 License.





Supplement of

Accelerated phosphorous leaching during abrupt climate transitions in a temperate Atlantic ecosystem in Northwest Spain recorded by stalagmite P / Ca variations

Nicolas Tapia et al.

Correspondence to: Nicolas Tapia (nico.explorer@yahoo.com) and Heather Stoll (heather.stoll@eaps.ethz.ch)

The copyright of individual parts of the supplement might differ from the article licence.

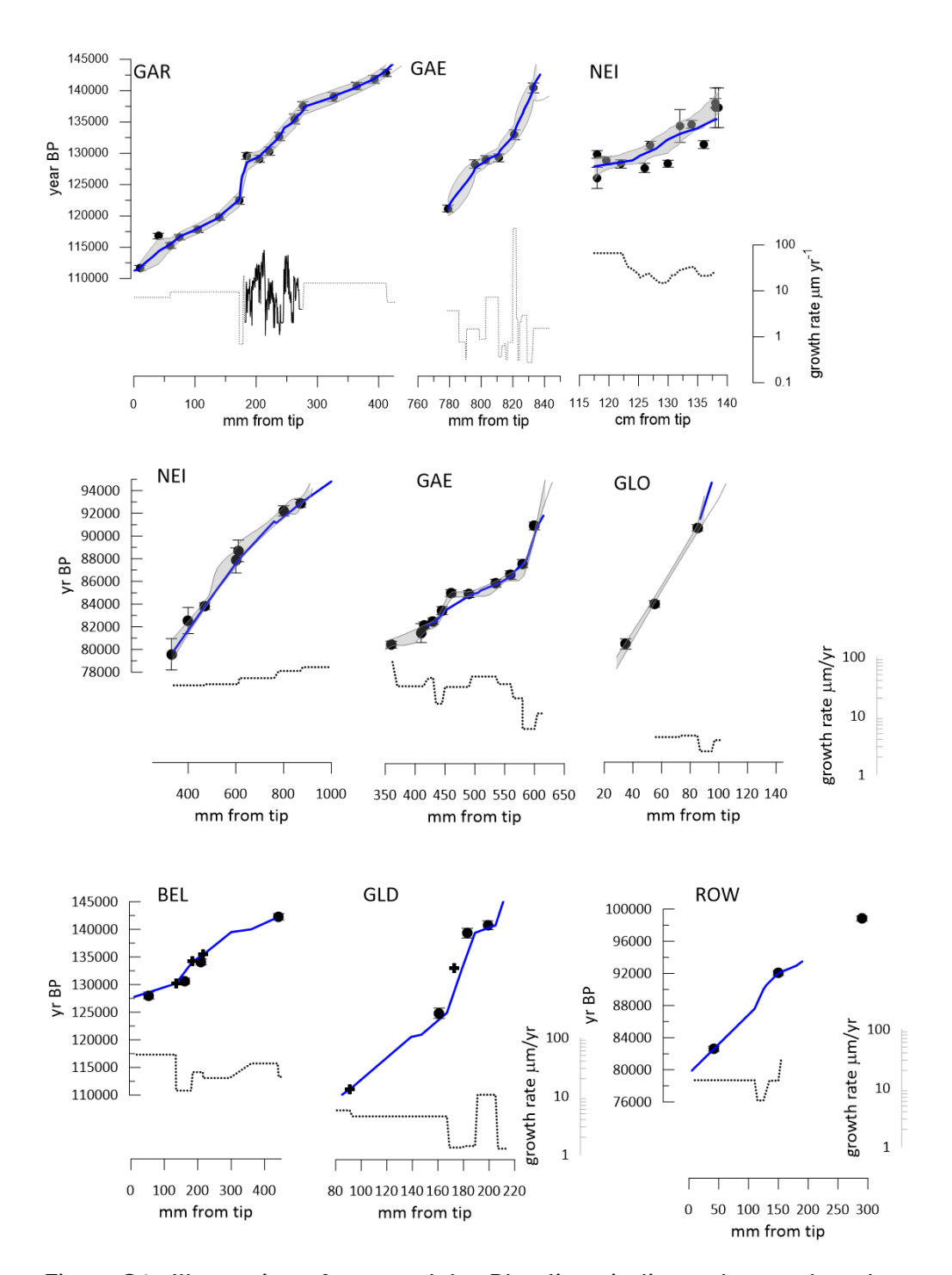


Figure S1. Illustration of age models. Blue lines indicate the employed age model. Gray shading illustrates the 95% confidence intervals for age models generated in BCHRON in top row, from (Stoll et al., 2022)) and in STALAGE in middle row, from (Stoll et al., 2015). Lower row illustrates age models from (Stoll et al., 2023). Growth rate estimated from the age models is shown in solid line for layer counted segments and dashed line for age models based on U/Th ages and tiepoints. Published U/Th dates are shown as circles with error on age assignments. For the lower row, tiepoints to isotope records in GAR (crosses) are also illustrated.

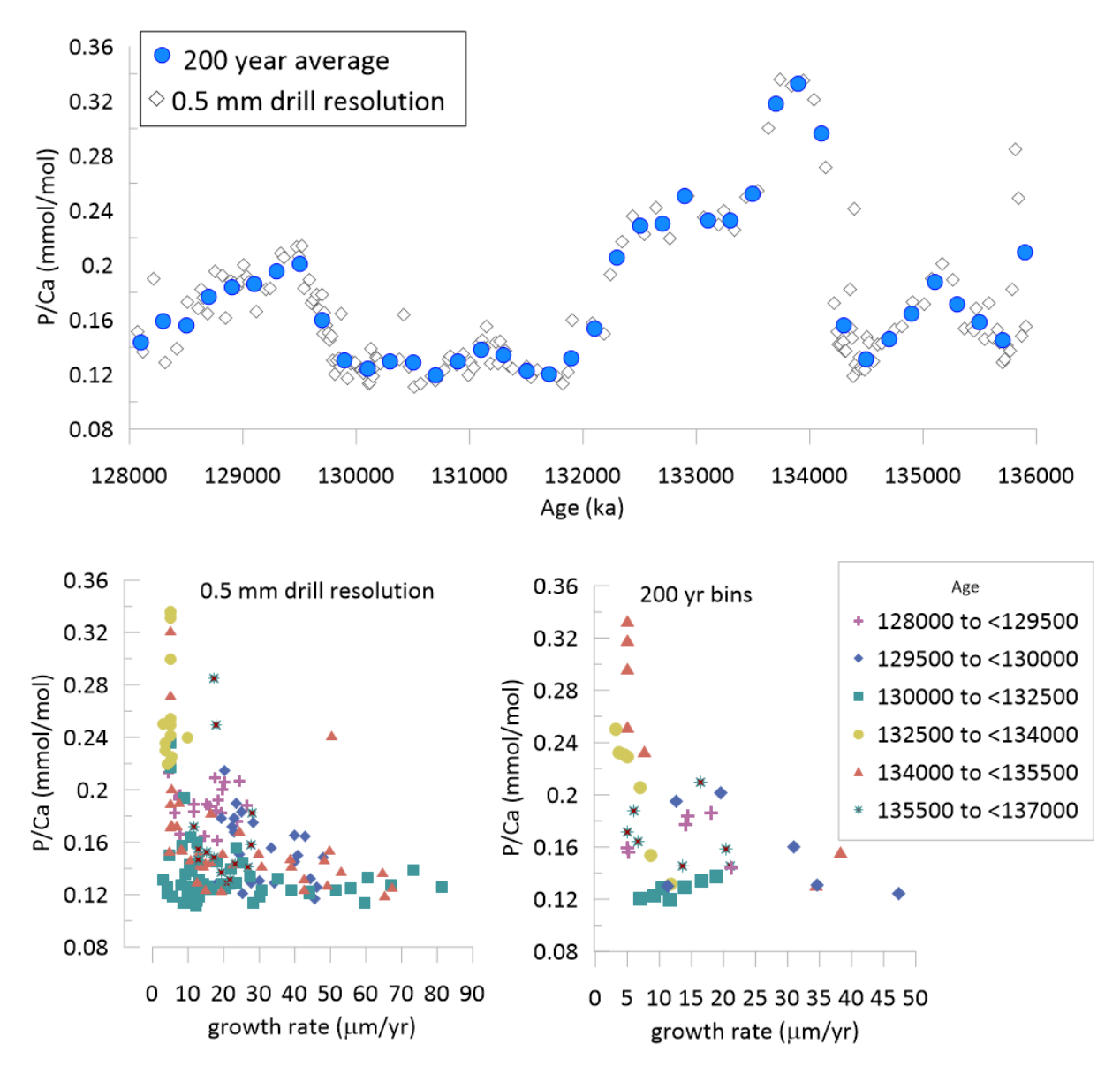


Figure S2. Upper panel shows, for the 136 to 128 ka interval with age model constrained by layer counting in GAR, the P/Ca for Garth for each drilled sample (open diamonds) compared with the average P/Ca in 200 yr age bins (blue circles). The consistency of trends indicates that the transient peaks in P/Ca are not artifacts of different durations integrated by the drill samples due to variable growth rates (Figure S1) and layer thicknesses. Lower panels show the correlations in P/Ca ratios of samples classified by age. Because growth rate slows at the onset of stadial intervals, higher P/Ca are clustered in intervals of slower growth, but slow growth periods also feature low P/Ca.

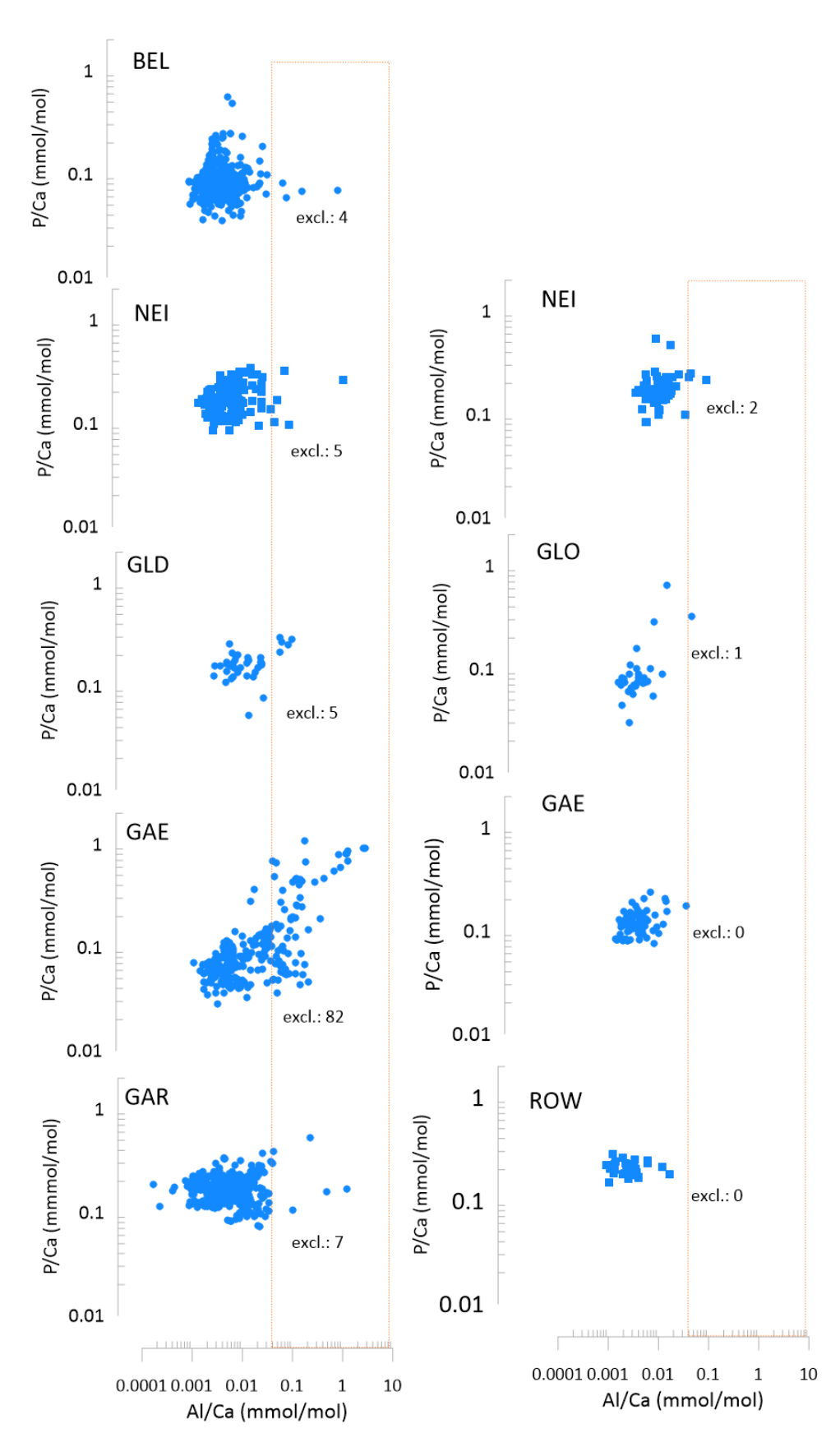


Figure S3. For each evaluated stalagmite, the measured P/Ca ratio vs Al/Ca ratio (mmol/mol). Left column shows results for PGM-LIG, and right column for GS 22. Text indicates the number of samples excluded from subsequent analyses due to exceeding the Al/Ca threshold criteria.

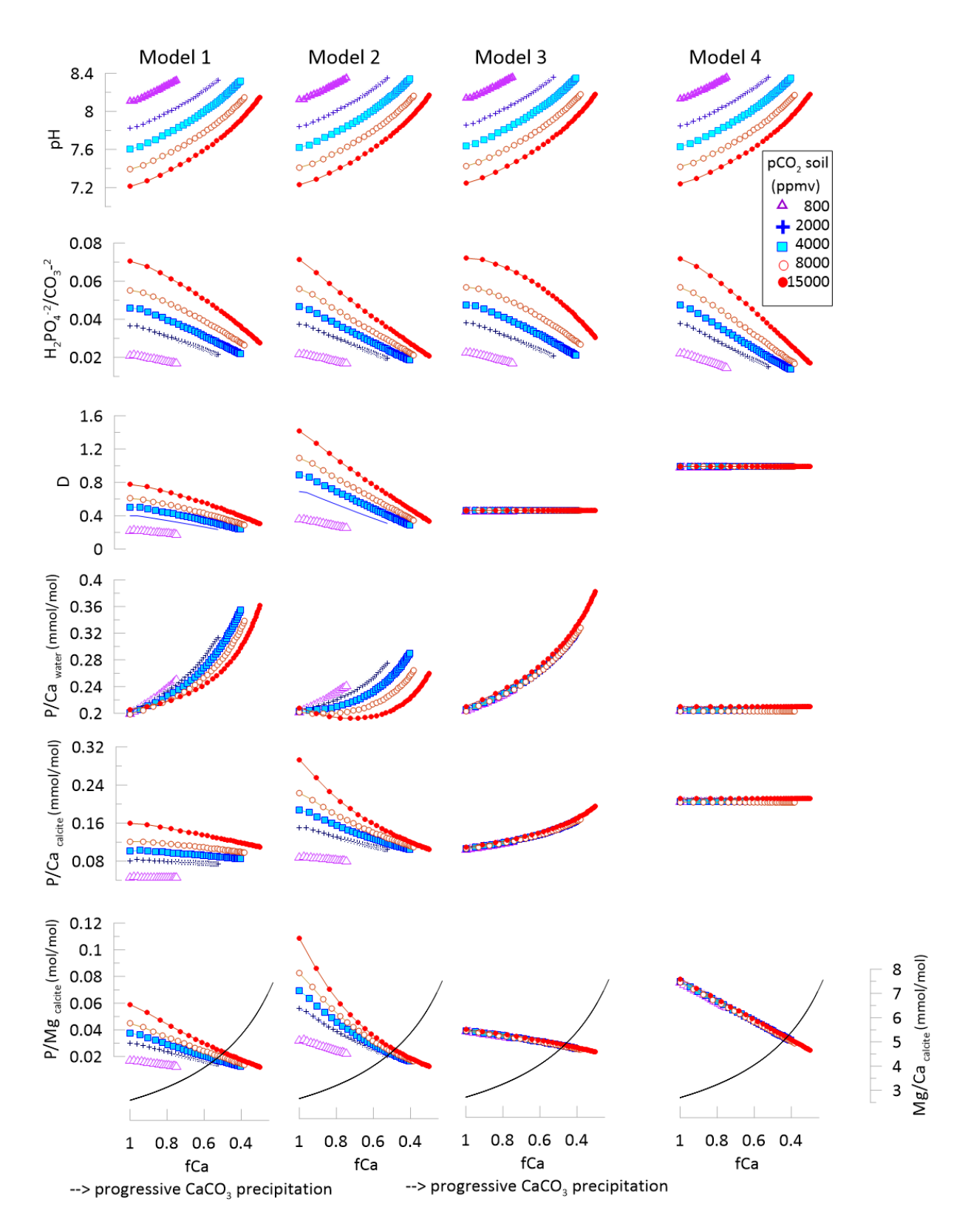


Figure S4. Simulations of the evolution of dripwater and stalagmite chemistry from initial dissolution through degassing and precipitation of calcite in the cave, for five different initial soil pCO2 dissolution scenarios given in Table S1. Evolution of dripwater pH and carbonate system parameters, Ca, and Mg is derived from CAVECALC simulations summarized in Table S1. In models 1 and 2, the phosphorus partitioning (D) depends on the solution ratio of HPO4–2 to CO3–2 , with maximum D of 0.76 and 1.4, respectively. In models 3 and 4, the phosphorus partitioning (D) is constant with value of 0.5 and 1, respectively. The Mg/Ca of calcite evolves identically with fCa in all scenarios and is illustrated with a black line in the lowermost models.

Results from Figure S4 and S5

For a constant P/Ca of drip water, our model calculations show significant variation in the P/Ca of the stalagmite due to the potential for changes in the P incorporation as a function of pH. Additionally, even for constant P incorporation, stalagmite P/Ca may vary due to evolution of the ratio of P/Ca and P to DIC species in the water.

Higher concentrations of soil and epikarst CO₂ leads to lower initial pH of drip water solutions, whereas successive degassing and calcite precipitation (higher fCa) lead to increased solution pH (Fig. S4). For the scenarios where the P incorporation in the calcite decreases in proportion to the solution ratio of HPO₄⁻² to CO₃⁻², there are two competing effects (Fig. S4, Model 1 and Model 2). On the one hand, the removal of P at a slower rate than Ca leads to increasing P/Ca (and P/DIC) ratio in the solution. At the same time, the increase in pH leads to increasing CO₃⁻² concentration which outpaces the increase in P/DIC, leading to a decrease in the solution ratio of HPO_4^{-2} to CO_3^{-2} . This decreases the partitioning of P in the calcite with increasing fCa. As a consequence, if D_{max} is 0.75 at pH 7.2, then the P/Ca ratio of calcite remains relatively stable regardless of the degree of degassing and calcite precipitation, but retains a strong effect of the initial drip water pH so that P/Ca ratios are nearly 3-fold higher for the case of 15000 ppmv soil pCO₂ compared to 800 ppmv (Fig. S4 Model 1). When the P incorporation in the calcite is higher (with D_{max} set as 1.46 at the lowest drip water pH of 7.2) and subsequently decreases in proportion to the solution ratio of HPO₄⁻² to CO₃⁻² (reaching a D of around 0.5 at pH 8), the rate of P removal is more comparable to that of Ca and DIC. Consequently, for the higher soil pCO₂ cases, there is a significant decrease in P/Ca with increasing fCa (Fig.S4 Model 2). For example, for Dmax = 1.46 and soil CO₂ of 4000 ppm, as fCa drops from 0.92 to 0.62, the P/Ca of calcite declines by about 30%. If the P incorporation is pH dependent (Dmax =0.75 or 1.46), then for a constant initial drip water P/Ca and constant fCa, the PCa will increase if the soil pCO₂ is higher (lower pH), which would be manifest by a negative correlation with δ^{13} C _{init} and PCa, with a halving of P/Ca as δ^{13} C_{init} falls from 12 to 8.5 % (Figure S5).

In contrast, if the P incorporation in the calcite is constant at 0.5 (Fig. S4 Model 3), then the soil pH has no effect on the P/Ca but there is a strong increase in the P/Ca with progressive degassing and calcite precipitation. For example, as fCa drops from 0.92 to 0.62, the P/Ca increases about 25%. If the P incorporation is constant (D=0.5), P/Ca is uncorrelated with $\delta^{13}C_{init}$ (Fig. S5). If the P incorporation is constant at D=0.5 then if drip water P/Ca is stable, P/Ca will be higher for a lower fCa. A change in fCa would lead to an inverse correlation between P/Ca and P/Mg, contrasting with the positive correlation due to change in initial dripwater P/Ca (Fig. S5).

If P incorporation in the calcite is constant at 1, then the P/Ca ratio is insensitive to both fCa and the initial soil pCO₂ (Fig. S4 Model 4). For a constant initial dripwater P/Ca, if D=1, then P/Ca does not vary with fCa but P/Mg does vary with fCa. For all cases, variation in the soil pCO₂ has no impact on the correlation between P/Ca and P/Mg (Fig.

S5). This tendency could be compensated in some stalagmites if an increase in soil pCO₂ (raising P/Ca) were accompanied by a lower fCa due to the higher drip water saturation (lowered P/Ca) (Fig. S5)

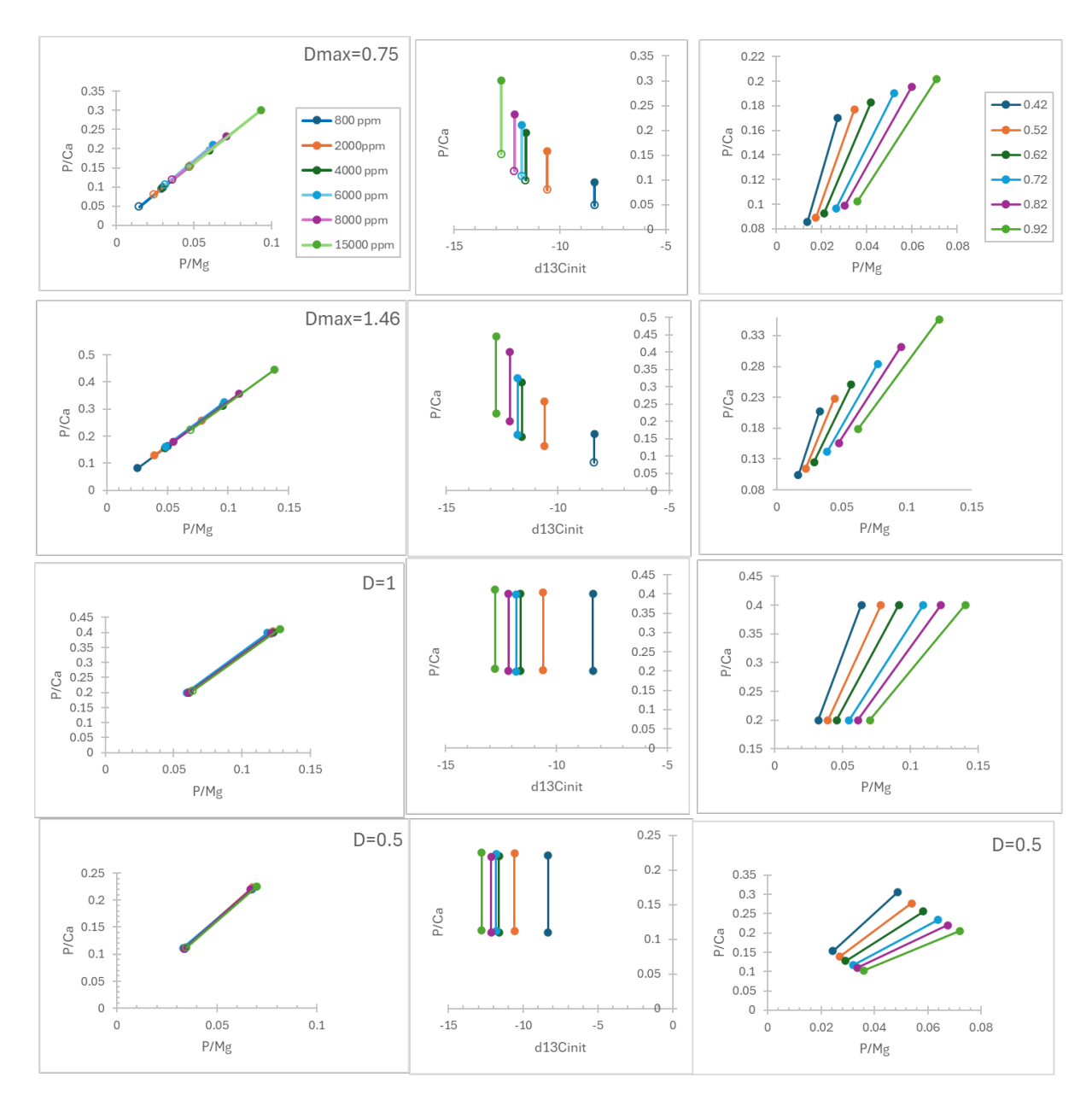


Figure S5. Illustration of stalagmite chemistry predicted from simulations shown in Figure S4, but comparing the effect of two ratios of initial dripwater P/Ca, 0.2 and 0.4 mmol/mol. The left two columns illustrate results for a constant fCa of 0.75 but varying initial soil pCO $_2$ and solid lines connect simulations of identical soil pCO $_2$ but different initial dripwater P/Ca. The rightmost column illustrates results for a constant soil pCO $_2$ of 4000 ppm but varying fCa, and solid lines connect simulations of identical fCa but different initial dripwater P/Ca. The δ^{13} C_{init} is estimated from CaveCalc simulations as described in the text.

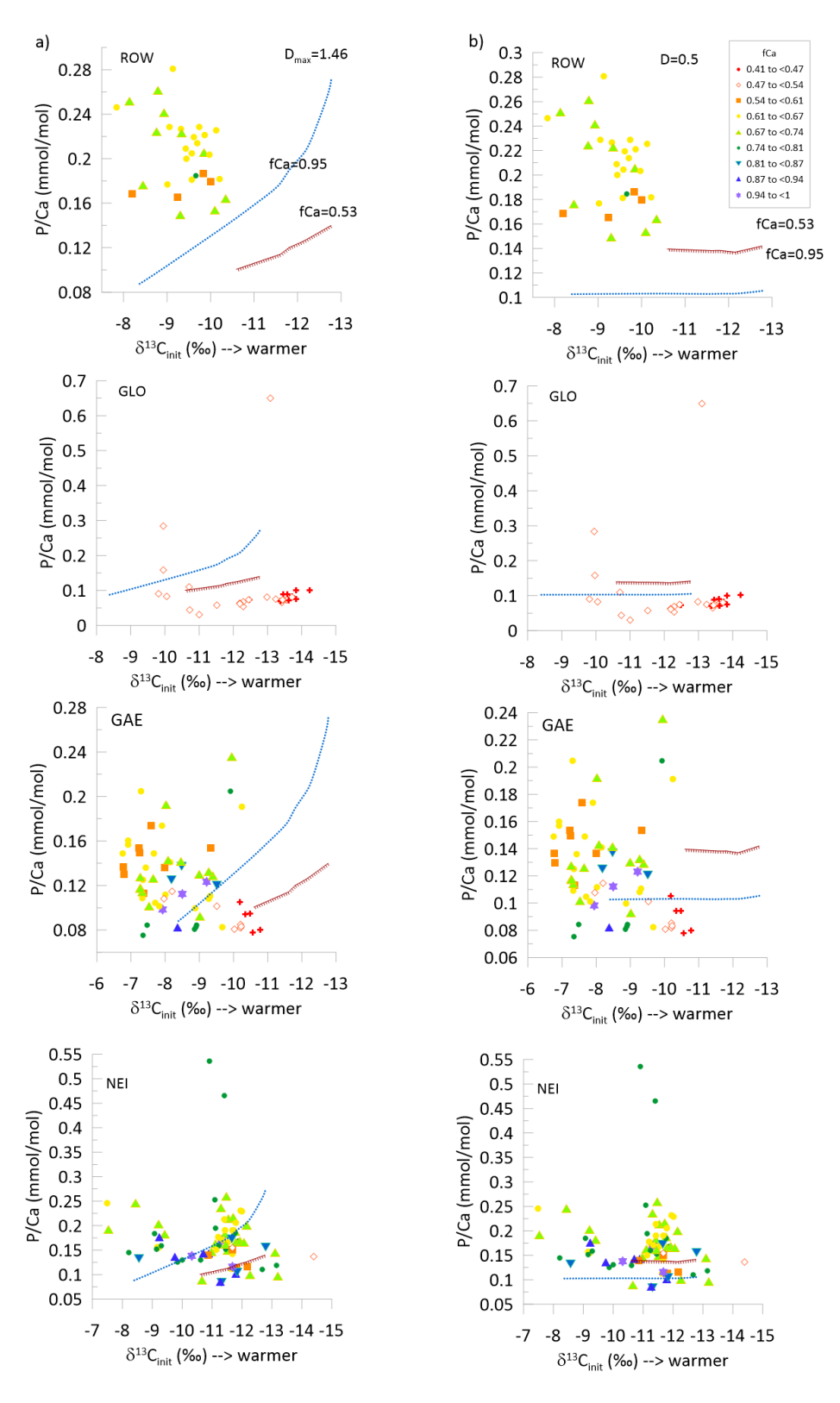


Figure S6. For the stalagmites covering the GS22 period, the P/Ca vs $\delta^{13}C_{init}$, with symbols indicating the fCa. Lines illustrate additionally the modeled variation of P/Ca with $\delta^{13}C_{init}$ for a dripwater of constant initial P/Ca (0.2 mmol/mol) for the case of fCa 0.95 and 0.52. Panel a) illustrates the results of model 1 where Dmax=1.46 and panel b) illustrates the results of model 3 where D=0.5.

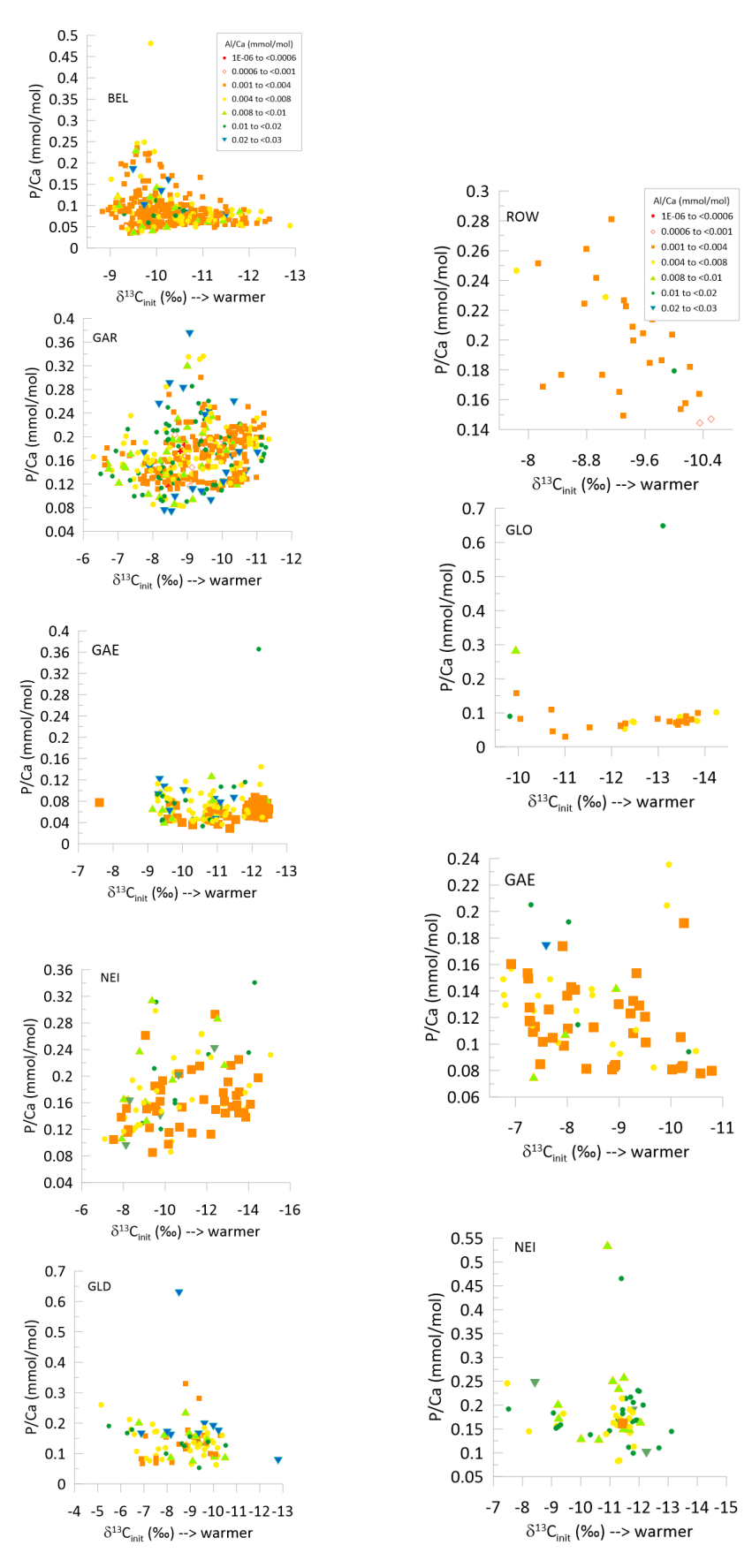


Figure S7. For each evaluated stalagmite, the measured P/Ca ratio vs variation in fCa , symbols coded with the measured Al/Ca ratio.

Table S1: Input parameters used in in the CAVECALC simulations.

| soil Gas pCO ₂ | Cave air pCO ₂ | Temperature °C | gas volume L |
|------------------------------|---------------------------|----------------|--------------------|
| 15000 | 550 | 13 | 150 |
| 8000 | 550 | 13 | 150 |
| 4000 | 300 | 9 | 150 |
| 2000 | 300 | 5 | 150 |
| 800 | 300 | 5 | 150 |

References

Stoll, H., Mendez-Vicente, A., Gonzalez-Lemos, S., Moreno, A., Cacho, I., Cheng, H., and Edwards, R. L.: Interpretation of orbital scale variability in mid-latitude speleothem δ 18 O: Significance of growth rate controlled kinetic fractionation effects, Quaternary Science Reviews, 127, 215-228, 2015.

Stoll, H. M., Day, C., Lechleitner, F., Kost, O., Endres, L., Sliwinski, J., Pérez-Mejías, C., Cheng, H., and Scholz, D.: Distinguishing the combined vegetation and soil component of δ 13 C variation in speleothem records from subsequent degassing and prior calcite precipitation effects, Climate of the Past, 19, 2423-2444, 2023.

Stoll, H. M., Cacho, I., Gasson, E., Sliwinski, J., Kost, O., Moreno, A., Iglesias, M., Torner, J., Perez-Mejias, C., and Haghipour, N.: Rapid northern hemisphere ice sheet melting during the penultimate deglaciation, Nature communications, 13, 1-16, 2022.